AIAA JOURNAL
Vol. 38, No. 2, February 2000

Two-Dimensional Elliptic Grid Solver Using Boundary Grid Control and Curvature Correction

Yih Nen Jeng* and Wei Jin Kuo†
National Cheng-Kung University, Tainan 70101, Taiwan, Republic of China

The Thompson method of explicitly evaluating control function of the elliptic grid solver is employed to improve local grid quality around convex and concave boundaries. The curvature correction is principally added to the grid lines around a boundary and is quickly attenuated as the grid points move inward. The algebraic advancing front method is employed to estimate two levels of orthogonal grids for evaluating the control functions at the boundary. If the grid equation based on the Cauchy–Riemann relation with ξ and η as independent variables is employed, numerical examinations show that a lengthy trial-and-error procedure is required to get a satisfactory grid distribution. In contrast, the method based on the Cauchy–Riemann relation with x and y as independent variables, which benefits from the maximum principle, not only removes the undesired grid clustering and diluting easily but also effectively improves overall grid smoothness and slightly enhances boundary grid orthogonality.

Nomenclature

a_1, b_1, c_1, d_1	= user-specified parameters; see Eq. (9)
a_2, b_2, c_2, d_2	= user-specified parameters; see Eq. (9)
f	= $1/r$ the curvature
$\boldsymbol{i}, \boldsymbol{j}, \boldsymbol{k}$	= unit vectors in the x, y, z directions, respectively
J	= Jacobian; see Eq. (2)
m	= modification factor of ϕ, ψ; Eq. (28)
P, Q	= control function of Eq. (3)
R_1, R_2	= functions of Eqs. (5b) and (23–25)
r	= radius of curvature
s	= arc length
x, y	= coordinates on the physical domain
α, β, γ	= functions defined in Eq. (2)
θ	= grid angle
κ	= curvature; Eq. (14)
ν	= $\leq \frac{1}{2}$, parameter of Eq. (17)
ξ, η	= coordinates on the computational domain
ϕ, ψ	= control functions; Eq. (4)
ω, ω_1	= user-specified parameters; see Eq. (16)

Subscripts

i, j	= grid indices along ξ, η direction, respectively
o	= variables on boundary
ξ, η	= partial derivatives, $x_\xi = \partial x/\partial \xi$, $x_\eta = \partial x/\partial \eta, \ldots$

Introduction

IN the recent past two popular methods for generating grid systems have been developed.[1] The first method involves solving elliptical, parabolic, or hyperbolic partial differential equations; the second method employs algebraic formulas. The elliptical equation method[1–7] can easily preserve grid smoothness over the entire domain. Moreover, unlike the other methods, the user-friendly elliptical equation method requires very little preprogramming and can generate a satisfactory grid system without requiring much practice. Therefore, the elliptical equation method is the most popular of all of the structure grid generation methods, even though it requires a much longer computing time.

The earliest literature regarding the second-order elliptical equation method of structure grid generation is the Laplace equation method of Winslow.[8] He employed the Laplace equation as the grid equations that employed the coordinates on the computational domain as dependent variables to preserve the benefit of the maximum principle. To gain the benefit of conveniently specifying the body-fitted boundary condition, he also proposed to swap the dependent and independent variables. In 1974 Thompson et al. added source terms to the grid equation of Ref. 8 to control grid distribution in the interior region[1–7,9,10] and developed the well-known TOMCAT program. Because the control function of Thompson et al. employs coordinates of the computational domain as independent variables, the adjustment of grid clustering and diluting is not a direction method. Researchers have to estimate the grid location on the physical domain before obtaining the desired location of grid clustering and diluting.

In 1979 Steger and Sorenson proposed the control method for boundary grid size and orthogonality[1–5,11–15] and developed the GRAPE program. They evaluated the implicit control function on the boundary-from-boundary and interior data. Subsequently, an exponential function is employed to find the control function in the interior points. To enhance the convergence, they designed a limited function to restrict the variation for control functions. Because the factors of the interpolation of the exponential function are related to both the convergence of the iterative procedure and final grid distribution, the user's experience is important in the complicated region. Hsu and Lee[15] pointed out that the method by which Steger and Sorenson distribute the control function is not an interpolation formula and proposed the one-dimensional interpolation formula. Jeng and Liou employed the two-dimensional transfinite interpolation formula for the control function.[16,17]

In 1980 Thomas and Middlecoff proposed a direct method for grid control on boundaries.[18] They rewrote the grid equations and noted that for two-dimensional grid systems one control function is closely related to the grid size distribution along one family of grid lines, and the other control function is related to the grid size distribution along another family. After making proper assumptions, they evaluated one control function explicitly along one pair of opposite boundaries and the other control function along the other pair. Because their method does not require iteration of the control function, the convergent problem does not occur, making this method preferred for two and three dimensions. According to the authors' experience, however, grid controllability suffers at concave and convex regions along a boundary. Around a concave corner of a boundary (such as the upper corner of a backward-facing step flow region), grid lines cluster in the corner. Likewise, grid lines move away from the corner, around convex corners (such as the lower corner of the backward-facing step region). Obviously, a grid control via distribution along boundaries stemming from two ends of the boundary is seriously distorted in these regions.

Received 13 November 1997; revision received 21 June 1999; accepted for publication 8 July 1999.

*Professor, Department and Institute of Aeronautics and Astronautics; ynjeng@mail.iaa.ncku.edu.tw. Member AIAA.

†Graduate Student, Department and Institute of Aeronautics and Astronautics.

Recently, three fast-advancing front methods of grid generation have been proposed: the algebraic method,[19] the hyperbolic equation method,[20] and the parabolic equation method.[21] All of these methods are principally designed to simulate the elliptic equation method. To eliminate undesired grid clustering and diluting around sharp corners along a boundary, these methods include enhancements involving user-specified parameters. Once the method does not function, researchers must obtain a proper set of parameters through a trial-and-error procedure whose efficiency depends on user experience. If we learn how to eliminate the uncontrollability of the Thomas–Middlecoff method at the sharp corner, these fast-advancing front methods may be further improved so that their enhancements need not involve user-specified parameters.

In Ref. 16 the point was made that the Thomas–Middlecoff method does not involve the curvature terms along a boundary and cannot correctly control the grid size and grid angle along a boundary. Visbal and Knight[22] considered the curvature effect and proposed a predictor-corrector procedure to generate grids. Another method of generating an orthogonal grid system was first proposed by Ryskin and Leal,[23] who considered the ratio between scale factors as the grid control function. Their work was followed by a series of literature[24–28] that effectively generated the orthogonal grid system. An interesting approach is the composite transformation method proposed by Spekreijse[29] that involves an algebraic transformation between the computational domain and parameter space and an transformation (defined by the Laplace equation) between the parameter space and physical domain. The curvature terms are partially resolved by the algebraic transformation and partially by the Laplace equation.

In 1987 Thompson[30] had proposed a convenience manner to include curvature terms via the control function that can be determined by estimation or else. In this study Thompson's explicit method of specifying control function is employed to improve grid quality around sharp corners. Although similar improvement can be achieved by dividing the computational domain into multiple block system to remove the negative effect of the corner, the additional preprogramming work will deteriorate one of the merits of employing the elliptic grid solver that very little preprogramming is necessary.

Analysis

For the sake of completeness, related existing works are briefly restated next. Winslow[8] employed the Laplace equation as a grid equation where

$$\xi_{xx} + \xi_{yy} = 0, \qquad \eta_{xx} + \eta_{yy} = 0 \tag{1}$$

For the sake of specifying the body-fitted boundary condition in a convenient manner, he proposed to swap dependent and independent variables. The grid equations become

$$\alpha x_{\xi\xi} - 2\beta x_{\xi\eta} + \gamma x_{\eta\eta} = 0, \qquad \alpha y_{\xi\xi} - 2\beta y_{\xi\eta} + \gamma y_{\eta\eta} = 0$$
$$\alpha = x_\eta^2 + y_\eta^2, \qquad \beta = x_\xi x_\eta + y_\xi y_\eta$$
$$\gamma = x_\xi^2 + y_\xi^2, \qquad J = x_\xi y_\eta - x_\eta y_\xi \tag{2}$$

Thompson et al. added source terms to Eq. (1) and developed the well-known Thompson–Thames–Mastin (TTM) equations[1–7,9,10]

$$\alpha x_{\xi\xi} - 2\beta x_{\xi\eta} + \gamma x_{\eta\eta} + J^2(Px_\xi + Qx_\eta) = 0$$
$$\alpha y_{\xi\xi} - 2\beta y_{\xi\eta} + \gamma y_{\eta\eta} + J^2(Py_\xi + Qy_\eta) = 0 \tag{3}$$

where P, Q are density control functions. Thomas and Middlecoff transformed the P, Q functions into ϕ, ψ and modified the grid equations to be

$$\alpha(x_{\xi\xi} + \phi x_\xi) - 2\beta x_{\xi\eta} + \gamma(x_{\eta\eta} + \psi x_\eta) = 0$$
$$\alpha(y_{\xi\xi} + \phi y_\xi) - 2\beta y_{\xi\eta} + \gamma(y_{\eta\eta} + \psi y_\eta) = 0$$
$$P = \phi(\xi, \eta)(\xi_x^2 + \xi_y^2), \qquad Q = \psi(\xi, \eta)(\eta_x^2 + \eta_y^2) \tag{4}$$

This study uses the notation of ϕ, ψ rather than P, Q.

Steger and Sorenson[11–16] assumed that, along an $\eta = 0$ boundary, grid size $[(s_\eta)_o = \mathrm{d}s/\mathrm{d}\eta|_o]$ and the angle (θ_o) of grid lines intersecting this boundary are known. After properly defining the first-order and second-order derivatives along the grid line, the control functions ϕ, ψ on the $\eta = 0$ boundary are

$$\phi_o = \left[\frac{-R_1 y_\eta + R_2 x_\eta}{\alpha J}\right]_o, \qquad \psi_o = \left[\frac{R_1 y_\xi - R_2 x_\xi}{\gamma J}\right]_o \tag{5a}$$

where

$$R_1 = [\alpha x_{\xi\xi} - 2\beta x_{\xi\eta} + \gamma x_{\eta\eta}]_o, \qquad R_2 = [\alpha y_{\xi\xi} - 2\beta y_{\xi\eta} + \gamma y_{\eta\eta}]_o \tag{5b}$$

Jeng and Liou[16,17] employed the following transfinite interpolation formula to evaluate the interior ϕ, ψ.

$$\begin{aligned}\phi(\xi, \eta) = {} & \left[\phi(\xi, 0)\left(1 - \frac{\eta}{\eta_{\max}}\right)^{a_1} + \phi(\xi, \eta_{\max})\left(\frac{\eta}{\eta_{\max}}\right)^{b_1}\right] \\ & + \left[\phi(0, \eta)\left(1 - \frac{\xi}{\xi_{\max}}\right)^{c_1} + \phi(\xi_{\max}, \eta)\left(\frac{\xi}{\xi_{\max}}\right)^{d_1}\right] \\ & - \left\{\left[\phi(0, 0)\left(1 - \frac{\eta}{\eta_{\max}}\right)^{a_1} + \phi(0, \eta_{\max})\left(\frac{\eta}{\eta_{\max}}\right)^{b_1}\right]\right. \\ & \times \left(1 - \frac{\xi}{\xi_{\max}}\right)^{c_1} + \left[\phi(\xi_{\max}, 0)\left(1 - \frac{\eta}{\eta_{\max}}\right)^{a_1}\right. \\ & \left.\left. + \phi(\xi_{\max}, \eta_{\max})\left(\frac{\eta}{\eta_{\max}}\right)^{b_1}\right]\left(\frac{\xi}{\xi_{\max}}\right)^{d_1}\right\}\end{aligned} \tag{6}$$

The ψ uses a similar interplant. These equations will be employed to evaluate interior ϕ, ψ for examples in this study on grid orthogonality.

Thomas and Middlecoff[18] explicitly evaluated the ϕ function along $\eta = 0$ and $\eta_{\max}$ boundaries and ψ along $\xi = 0$ and $\xi_{\max}$ boundaries. For example, along an $\eta = 0$ boundary they assumed that the grid orthogonality is preserved and grid lines intersecting the boundary are locally straightened. Consequently, the ϕ function is estimated from the following equation:

$$\phi_o = -\frac{x_\xi x_{\xi\xi} + y_\xi y_{\xi\xi}}{x_\xi^2 + y_\xi^2} \tag{7}$$

Along the other boundaries the corresponding control functions are evaluated in a similar manner. Finally, the interior control functions are evaluated via linear interpolation from data along the corresponding pair of opposite boundaries.

Proposed Methods

Starting from the Cauchy–Riemann conditions

$$x_\xi = y_\eta, \qquad x_\eta = -y_\xi \tag{8}$$

the following Laplace equations are easily obtained:

$$x_{\xi\xi} + x_{\eta\eta} = 0, \qquad y_{\xi\xi} + y_{\eta\eta} = 0 \tag{9}$$

For convenience, this equation and the corresponding modifications are called linear equations in this work, whereas the transformed equations of Winslow [Eq. (2)] and the corresponding modifications are called nonlinear equations. First, the Thomas and Middlecoff method is applied to the preceding equations to obtain

$$x_{\xi\xi} + \phi x_\xi + x_{\eta\eta} + \psi x_\eta = 0, \qquad y_{\xi\xi} + \phi y_\xi + y_{\eta\eta} + \psi y_\eta = 0 \tag{10}$$

Note that these linear equations can be obtained from Eq. (4) by setting $\alpha = \gamma = 1$ and $\beta = 0$. Following the derivation of Thomas

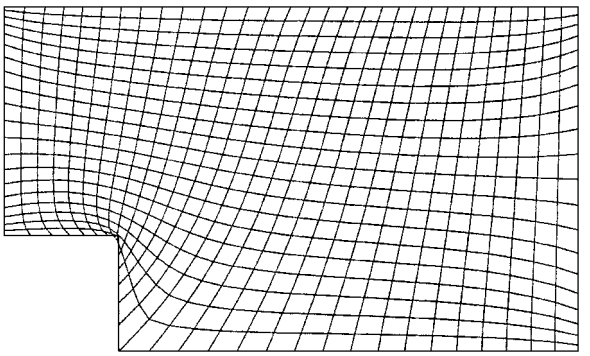

Fig. 1 Resulting grids in the backward-facing step region, generated by the Laplace equation of Eq. (9).

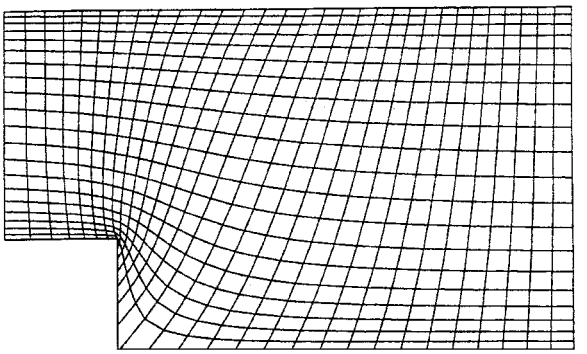

Fig. 2 Resulting grids in the backward-facing step region, generated by the Thomas and Middlecoff method.

and Middlecoff,[18] on the $\eta=0$ boundary the equation for the ϕ function is Eq. (7).

Now the Thomas and Middlecoff method and its linear version [defined by Eqs. (7) and (10)] are employed to solve the grid system for a backward-facing step flow region. The resulting linear and nonlinear grids are shown in Figs. 1 and 2, respectively. In the upper step corner both methods cause grid-line clustering near the corner. Both methods also draw grid lines away from the the lower step corner. As mentioned in the Introduction, these drawbacks come from missing the curvature effect in the bottom boundary.

Obviously, the linear grids have grid-line overspill even at the corner, as shown in Fig. 1. This can be explained by the fact that Eq. (9) does not have the maximum principle. The monotone grid distribution of Fig. 2 around the same region shows that the original Thomas and Middlecoff method is benefited from the maximum principle of Eq. (1).

Although the approach proposed by Ryskin and Leal[23–28] might resolve the grid overlapping of Fig. 1, the explicit Thompson method[30] is employed here. Consider a polar coordinate system where $\xi=\rho\theta$ and $\eta=\rho$. The relationship between (x, y) and (ξ, η) transforms the mapping from a fan-shape grid system to rectangular grids. Let us substitute Eq. (9) with

$$(1/\rho^2)x_{\theta\theta} + x_{\rho\rho} + (1/\rho)x_\rho = 0$$
$$(1/\rho^2)y_{\theta\theta} + y_{\rho\rho} + (1/\rho)y_\rho = 0 \qquad (11)$$

By recognizing that along ξ direction $\rho=$constant and setting $d\xi=-\rho\, d\theta$, Eq. (11) is rewritten as

$$x_{\xi\xi} + x_{\eta\eta} + (1/\rho)x_\eta = 0, \qquad y_{\xi\xi} + y_{\eta\eta} + (1/\rho)y_\eta = 0 \qquad (12)$$

which is a special case of the Thompson method with uniform grid distribution along η direction.

Although the conceptual starting point of Thompson differs, we believe that the following discussion does not lose generality. Assume that around point (i, j), $x_{i+\ell, j+m}=(r_o+m\delta r_o)\cos(\theta+\ell\delta\theta)$, $y_{i+\ell, j+m}=(r_o+m\delta r_o)\sin(\theta+\ell\delta\theta)$ where local uniform mesh distribution with $\Delta\xi=r_o\delta\theta=\Delta\eta=\delta r_o\ll 1$ is employed, as shown in Fig. 3, then

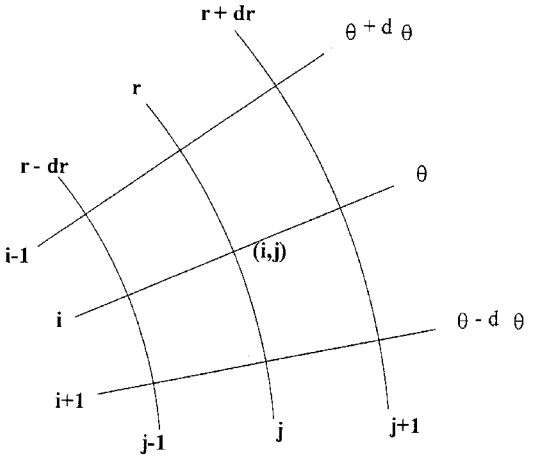

Fig. 3 Schematic diagram of a polar-coordinate-type grid point distribution.

$$x_{\xi\xi} \sim \frac{x_{i+1,j} - 2x_{i,j} + x_{i-1,j}}{r_o^2\delta^2\theta}$$
$$\sim \frac{1}{r_o^2\delta^2\theta}[r_o\cos(\theta-\delta\theta) - 2r_o\cos\theta + r_o\cos(\theta+\delta\theta)]$$
$$\sim -\frac{\cos\theta}{r_o}$$
$$\frac{1}{\rho}x_\eta \sim \frac{x_{i,j+1} - x_{i,j-1}}{2r_o\Delta\eta} \sim \frac{1}{2r_o^2\delta\theta}[(r_o+\delta r_o)\cos\theta - (r_o-\delta r_o)\cos\theta]$$
$$\sim \frac{2r_o\delta\theta\cos\theta}{2r_o^2\delta\theta} = \frac{\cos\theta}{r_o}$$
$$x_{\eta\eta} \sim \frac{x_{i,j+1} - 2x_{i,j} + x_{i,j-1}}{\Delta^2\eta}$$
$$\sim \frac{1}{2r_o^2\delta\theta}[(r_o+\delta r_o)\cos\theta - 2r_o\cos\theta + (r_o-\delta r_o)\cos\theta] \sim 0 \qquad (13)$$

Similarly

$$y_{\xi\xi} \sim -\sin\theta/r_o, \qquad (1/\rho)y_\eta \sim \sin\theta/r_o, \qquad y_{\eta\eta} \sim 0 \qquad (14)$$

The preceding analysis shows that, in a perfect polar-coordinate-type grid system, $x_{\xi\xi}$ and $y_{\xi\xi}$ are canceled by $(1/\rho)x_\eta$ and $(1/\rho)y_\eta$, respectively, whenever $\delta\theta\to 0$.

In a generalized grid system a fan-shaped grid distribution around a corner might not be a good choice because the desired curvature might be changed point to point, which means that the curvature cannot be estimated easily. Therefore, this study employs the following strategies:

1) The curvature correction should satisfy the following requirements:

$$x_{\xi\xi} + (1/\rho)x_\eta \sim 0, \qquad y_{\xi\xi} + (1/\rho)y_\eta \sim 0 \qquad (15)$$

2) The curvature around the boundaries is evaluated and rapidly attenuated as points move toward the interior region.

3) The curvature in the interior region is replaced by the smoothing effect of the elliptic equation.

For the first requirement the curvature $1/\rho$ is approximated as

$$\frac{1}{\rho} = f = \omega_1\kappa = \omega_1\sqrt{\left(\frac{d^2x}{d\xi^2}\right)^2 + \left(\frac{d^2y}{d\xi^2}\right)^2}\Bigg/ \; s_\eta \qquad (16)$$

$$\omega_1 = \omega\frac{\boldsymbol{r}^+\times\boldsymbol{r}^-}{|\boldsymbol{r}^+||\boldsymbol{r}^-|}, \qquad \boldsymbol{r}^+ = (x_{i+1,j} - x_{i,j})\boldsymbol{i} + (y_{i+1,j} - y_{i,j})\boldsymbol{j}$$
$$\boldsymbol{r}^- = (x_{i,j} - x_{i-1,j})\boldsymbol{i} + (y_{i,j} - y_{i-1,j})\boldsymbol{j}$$

where the term $\boldsymbol{r}^+ \times \boldsymbol{r}^- / |\boldsymbol{r}^+||\boldsymbol{r}^-|$ is employed to involve the effect of the grid size and grid angle between two successive grid segments.

To obtain fast-attenuated curvature terms, the interior function f of Eq. (16) is evaluated by solving the Laplace equation or linear parabolic equation. If only one boundary requires the curvature correction, the following implicit differenced parabolic equation is employed:

$$f_{i,j+1} = f_{i,j} + \nu(f_{i+1,j+1} - 2f_{i,j} + f_{i-1,j+1}) \tag{17}$$

where $j+1$ is the advanced grid level. If more than one boundary requires curvature correction, the following differenced Laplace equation is iteratively solved several times by the successive line underrelaxation (SLUR) method:

$$f_{i+1,j} + f_{i-1,j} + f_{i,j+1} + f_{i,j-1} - 4f_{i,j} = 0 \tag{18}$$

If grid control is necessary, Eqs. (12) become

$$\begin{aligned} x_{\xi\xi} + \phi x_\xi + x_{\eta\eta} + [\psi + 1/\rho(\eta)]x_\eta = 0 \\ y_{\xi\xi} + \phi y_\xi + y_{\eta\eta} + [\psi + 1/\rho(\eta)]y_\eta = 0 \end{aligned} \tag{19}$$

Compared to Eq. (10), the possibility of grid overlapping is significantly reduced, provided that the grid distribution should be made locally similar to a polar grid system. Otherwise, the curvature correction cannot compensate for the oversmoothing introduced by $()_{\xi\xi}$.

When the grid system is governed by Eq. (1), the maximum principle introduces a positive effect that preserves grid monotonicity at concave corners. If the curvature correction is added to Eq. (1), grid controllability can be effectively enhanced. Around the $\eta = 0$, $\eta_{\max}$ boundary let $\xi \sim \rho\theta$, $\eta \sim \rho$ and introduce grid control functions; Eq. (1) locally takes the following form:

$$\begin{aligned} \frac{\partial}{\partial x}\left(\rho\frac{\partial \theta}{\partial x}\right) + \frac{\partial}{\partial y}\left(\rho\frac{\partial \theta}{\partial y}\right) = P \\ \frac{\partial}{\partial x}\left(\frac{1}{\rho}\frac{\partial \rho}{\partial x}\right) + \frac{\partial}{\partial y}\left(\frac{1}{\rho}\frac{\partial \rho}{\partial y}\right) = \frac{Q}{\rho} \end{aligned} \tag{20}$$

By interchanging the dependent and independent variables and using ϕ, ψ to represent P, Q, the preceding equations are transformed to become

$$\begin{aligned} &\alpha\left\{x_{\xi\xi} + \left[\phi + \frac{1}{\rho(\eta)}\frac{\beta}{\alpha}\right]x_\xi\right\} - 2\beta x_{\xi\eta} \\ &\quad + \gamma\left\{x_{\eta\eta} + \left[\psi + \frac{1}{\rho(\eta)}\right]x_\eta\right\} = 0 \\ &\alpha\left\{y_{\xi\xi} + \left[\phi + \frac{1}{\rho(\eta)}\frac{\beta}{\alpha}\right]y_\xi\right\} - 2\beta y_{\xi\eta} \\ &\quad + \gamma\left\{y_{\eta\eta} + \left[\psi + \frac{1}{\rho(\eta)}\right]y_\eta\right\} = 0 \end{aligned} \tag{21}$$

If all four boundaries should consider the curvature effect, the governing equations are

$$\begin{aligned} &\alpha\left\{x_{\xi\xi} + \left[\phi + \frac{1}{\rho(\xi)} + \frac{1}{\rho(\eta)}\frac{\beta}{\alpha}\right]x_\xi\right\} - 2\beta x_{\xi\eta} \\ &\quad + \gamma\left\{x_{\eta\eta} + \left[\psi + \frac{1}{\rho(\eta)} + \frac{1}{\rho(\xi)}\frac{\beta}{\gamma}\right]x_\eta\right\} = 0 \\ &\alpha\left\{y_{\xi\xi} + \left[\phi + \frac{1}{\rho(\xi)} + \frac{1}{\rho(\eta)}\frac{\beta}{\alpha}\right]y_\xi\right\} - 2\beta y_{\xi\eta} \\ &\quad + \gamma\left\{y_{\eta\eta} + \left[\psi + \frac{1}{\rho(\eta)} + \frac{1}{\rho(\xi)}\frac{\beta}{\gamma}\right]y_\eta\right\} = 0 \end{aligned} \tag{22}$$

where $\rho(\xi)$ designs the radius of the curvature aligning with the ξ-grid lines around the $\xi = 0$ or $\xi_{\max}$ boundary and $\rho(\eta)$ designs the radius of curvature aligning with the η-grid lines around the $\eta = 0$ or $\eta_{\max}$ boundary. Because $1/\rho(\xi)$ is zero at points remote from $\xi = 0$ and $\xi_{\max}$ boundaries and $1/\rho(\eta)$ is zero at locations remote from $\eta = 0$ and $\eta_{\max}$ boundaries, these curvature terms do not exist simultaneously except at the four corner points. Note that the preceding curvature correction can be considered to be the additional terms of the control function ϕ, ψ.

If the approximated grid orthogonality should be preserved, the control function of Steger and Sorenson should be employed. To guarantee the convergence of iteration, this study examines the method where the control function is not iteratively solved. Because of the explicit form of the control functions, the following procedure is referred to as the modified Thomas and Middlecoff methods. Suppose that the curvature correction along the $\eta = 0$ boundary is desired, which corresponds to the problem of Fig. 1. By performing proper algebraic manipulations, Eq. (19) gives the boundary ϕ, ψ as

$$\begin{aligned} \phi_o = [(-R_1 y_\eta + R_2 x_\eta)/J]_o, \qquad \psi_o = [(R_1 y_\xi - R_2 x_\xi)/J]_o \\ R_1 = \{x_{\xi\xi} + x_{\eta\eta} + [1/\rho(\eta)]x_\eta\}_o \\ R_2 = \{y_{\xi\xi} + y_{\eta\eta} + [1/\rho(\eta)]y_\eta\}_o \end{aligned} \tag{23}$$

In this study the algebraic advancing front method of Ref. 19 is employed to estimate two levels of grids, and hence ϕ_o, ψ_o, are known.

Corresponding to the nonlinear equations (21) and (22), Eq. (8b) takes the following forms, respectively:

$$\begin{aligned} R_1 &= \left\{\alpha\left[x_{\xi\xi} + \frac{1}{\rho(\eta)}\frac{\beta}{\alpha}x_\xi\right] - 2\beta x_{\xi\eta} + \gamma\left[x_{\eta\eta} + \frac{1}{\rho(\eta)}x_\eta\right]\right\}_o \\ R_2 &= \left\{\alpha\left[y_{\xi\xi} + \frac{1}{\rho(\eta)}\frac{\beta}{\alpha}y_\xi\right] - 2\beta y_{\xi\eta} + \gamma\left[y_{\eta\eta} + \frac{1}{\rho(\eta)}y_\eta\right]\right\}_o \end{aligned} \tag{24}$$

$$\begin{aligned} R_1 = \Bigg(&\alpha\left\{x_{\xi\xi} + \left[\frac{1}{\rho(\xi)} + \frac{1}{\rho(\eta)}\frac{\beta}{\alpha}\right]x_\xi\right\} - 2\beta x_{\xi\eta} \\ &+ \gamma\left\{x_{\eta\eta} + \left[\frac{1}{\rho(\xi)}\frac{\beta}{\gamma} + \frac{1}{\rho(\eta)}\right]x_\eta\right\}\Bigg)_o \\ R_2 = \Bigg(&\alpha\left\{y_{\xi\xi} + \left[\frac{1}{\rho(\xi)} + \frac{1}{\rho(\eta)}\frac{\beta}{\alpha}\right]y_\xi\right\} - 2\beta y_{\xi\eta} \\ &+ \gamma\left\{y_{\eta\eta} + \left[\frac{1}{\rho(\xi)}\frac{\beta}{\gamma} + \frac{1}{\rho(\eta)}\right]y_\eta\right\}\Bigg)_o \end{aligned} \tag{25}$$

If there is not significant curvature, the preceding method may be enough to partially preserve grid orthogonality. Otherwise, especially for the linear equation method of Eqs. (19), grid orthogonality may not be kept, and the curvature correction does not work properly. In such situations adjustment of the control functions is necessary to maintain grid orthogonality. For example, along an $\eta =$ constant line, the grid size Δs is related to ϕ function[31] via

$$s_{\xi\xi} + \phi_o s_\xi = 0 \tag{26}$$

Let $\Delta s \sim s_\xi$, so that the solution is

$$\Delta s = (\Delta s)_o e^{-\phi_o \xi} \tag{27}$$

According to this relation, at the ith point, Δs_i is increased as ϕ_o is made smaller and vice versa. Suppose a grid system is seriously distorted, either a larger or smaller control function will provide necessary adjustment.

Results and Discussion

Linear Grid System

To remedy the grid overlapping of Fig. 1, Eqs. (19) and (23) are employed to generate grids. In spite of correctly estimating ϕ, ψ via the algebraic advancing front method, the resulting grids do not

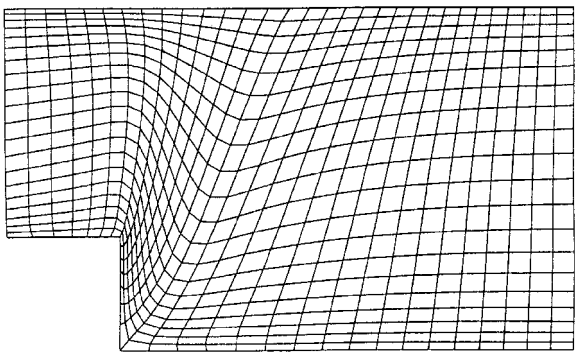

Fig. 4 Resulting grids in the backward-facing step region generated by Eq. (19) using curvature correction and grid adjustment of Eq. (28). Boundary ϕ, ψ are estimated by Eqs. (23) and the algebraic advancing front method.

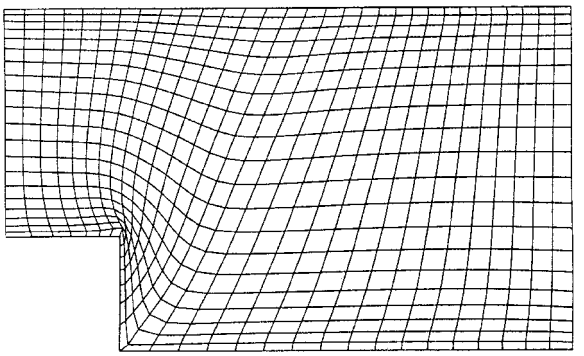

Fig. 5 Resulting grids of the backward-facing step region generated by Eqs. (5a), (7), (16), (21), (24), (29), and (30).

have grid overlapping but cannot avoid serious distortion around the upper corner of the lower boundary and is not shown here because of the content limitation. After a lengthy trial-and-error procedure, it is found that the following artificial increment of ϕ, ψ is helpful:

$$\phi_{i,j} = \phi_{i,j} - 0.6m, \qquad \psi_{i,j} = \psi_{i,j} + 0.17m \tag{28}$$

where

$$\begin{aligned} m &= 1/5^j \quad \text{for} \quad i = 5, \quad j = 1, 2, \ldots \\ &= 1/3^j \quad \text{for} \quad i = 7 \quad \text{upper step corner line} \\ &= -1/5^j \quad \text{for} \quad i = 9 \\ &= 0, \quad \text{otherwise} \end{aligned}$$

The resulting grid distribution is shown in Fig. 4. The grid overlapping is eliminated, and overall grid smoothness is attained. However, if the parameters 0.6 and 0.17 are changed more than 20%, grid distortion cannot be eliminated again. The authors have examined many other examples. Parameters giving satisfactory grid distribution are significantly different from each other and are very sensitive. Because of the limitation on length, they are not shown here.

Numerical tests show that the grid overlapping generated by linear equations can be effectively eliminated by the curvature correction only if grid orthogonality can simultaneously be preserved to a certain degree. However, the parameter range for preserving grid smoothness is very narrow and changes from case to case. Therefore, the linear equation method is not recommended.

Nonlinear Grid System

Figure 5 is the resulting grid distribution in the backward-facing step region generated by Eqs. (7) and (21), where the parameters of Eq. (16) are determined by

$$\omega = 6.8, \qquad \text{if} \quad \kappa \geq 1 \tag{29}$$

$$= 3, \qquad \text{if} \quad \kappa < 1 \tag{30}$$

The larger κ corresponds to an apex of a sharp corner, whereas the smaller κ is associated with a smooth boundary. Moreover, Eq. (17) with $\nu = 0.2$ is marched upward from the bottom boundary. Although the orthogonal condition is not considered, the maximum principle keeps grids from being seriously distorted so that grid orthogonality is preserved to a certain extent. Consequently, the curvature correction effectively eliminated the undesired grid clustering and dilution of Fig. 2. Figure 6 shows the comparison between the convergent histories of the absolute ℓ_2 residues, where the converging slopes of Figs. 2 and 5, respectively, are similar. Because the deviations between final grids and corresponding initial guesses (the same linear grids generated by the transfinite interpolation method) differ, the initial error of the present method is smaller, and hence the required CPU time is smaller.

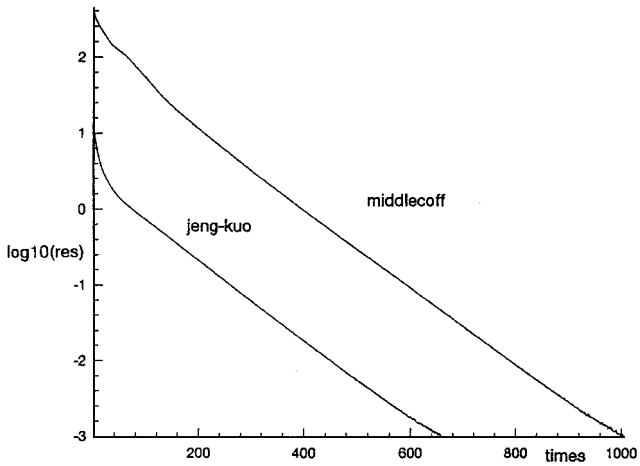

Fig. 6 Converging histories of Figs. 2 and 5, respectively.

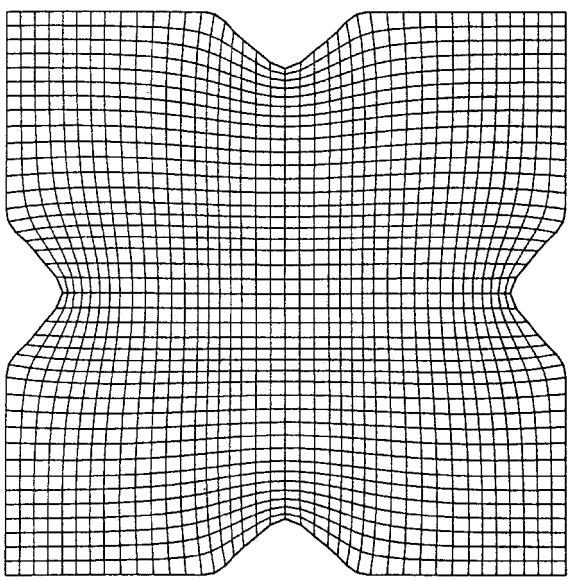

Fig. 7 Grid distribution in a smooth region generated by the Thomas and Middlecoff method.

Figures 7 and 8, two additional examples of grids generated through the original Thomas–Middlecoff method, show undesired grid imperfections similar to Fig. 2. Using the same parameter of Eqs. (16) and (17), Eqs. (7) and (22) generate grids of these two regions shown in Figs. 9 and 10, respectively. To distribute the curvature terms properly, Eq. (18) is solved in three cycles with an under-relaxation factor 0.2, where marching from the bottom to the top boundary and a marching from the left to the right boundary is counted as one cycle. In the region without any sharp corners along all of the boundaries, overall grid smoothness is attained, as shown in

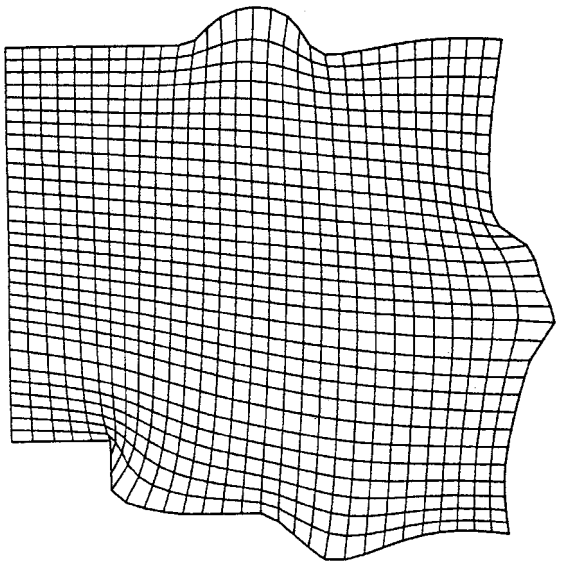

Fig. 8 Grid distribution in a relatively complicated region generated by the Thomas and Middlecoff method.

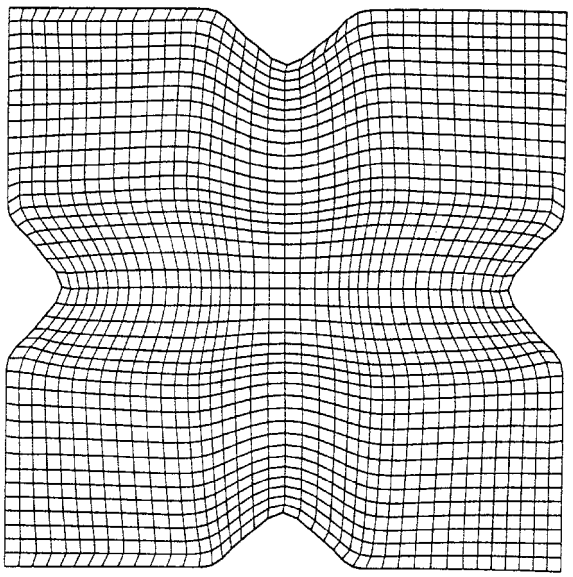

Fig. 9 Grid distribution in a smooth region generated by the method similar to that of Fig. 5.

Fig. 9. Figure 10 also shows similar grid smoothness except around the step corner.

Now the algebraic advancing front method of Ref. 19 is employed for generating two grid levels so that boundary ϕ, ψ can be estimated. The resulting grid system generated by the nonlinear modified Thomas and Middlecoff method [Eqs. (21), (29), and (30)] is shown in Fig. 11, where all of the data are the same as those of Fig. 5. The converging rate is nearly the same as that of Fig. 5 and is not shown here. It is surprising that grid smoothness is kept over the entire domain.

Results corresponding to Figs. 9 and 10 for the same modified Thomas and Middlecoff method, which considers grid orthogonality, are shown in Figs. 12 and 13, respectively. A careful examination of Figs. 7–13 reveals that employing a reasonable estimation of boundary ϕ, ψ obtains better boundary orthogonality around all of the boundaries and better grid smoothness over the entire domain.

For practical applications it is helpful to point out the range of the parameter ω of Eq. (16). At the smooth boundary point where $|f| = 1/\rho < 1$, numerical tests show that grid smoothness and approximated orthogonality can be easily achieved if $\omega \in (0, 3]$. At the sharp corner a wide range of ω is found as shown in the column of the

Table 1 Available range of ω of Eq. (14)[a]

Domain	Grid density	Lower-upper bounds	Range of smooth grids
Backward-facing step	31 ×20	0 ~ 11.2	4 ~ 10.5
Backward-facing step	62 ×40	0 ~ 9.2	4 ~ 8.5
Relatively complicated region	30 ×30	0 ~ 9	4.3 ~ 8.5
Relatively complicated region	60 ×60	0 ~ 7.5	4.5 ~ 7

[a]Note: The relatively complicated region corresponds to Fig. 8.

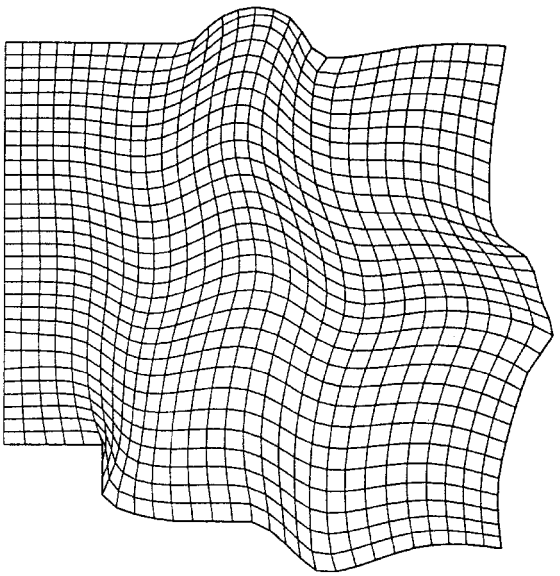

Fig. 10 Grid distribution in a relatively complicated region generated by the method similar to that of Fig. 5.

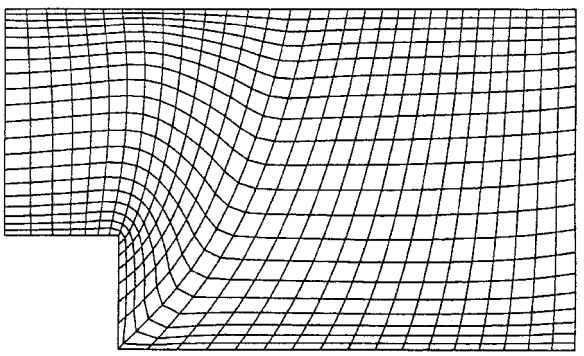

Fig. 11 Resulting grids of a backward-facing step, generated by Eqs. (5a), (7), (16), (21), (24), (29), and (30) and the algebraic advancing front method is employed to estimate boundary ϕ, ψ.

lower bounds to the upper bounds of Table 1. The range of smooth grids means that, with ω at this range, the resulting grid clustering or dilution at the corner is not significant and grid smoothness is preserved. If the grid is twice as dense, the lower bounds of both columns are nearly unchanged, and the upper bounds are slightly smaller. Consequently, if one defines the desired grid size distribution (including the desired grid clustering and dilution), an automatic search strategy can easily be designed to obtain the suitable value of ω.

The present study also compares the present curvature correction to the implicit control function method of Steger and Sorenson with Jeng and Liou's interpolation. No significant differences are found in the final grids and converging histories between two, and results are not shown here. In other words, if the iteration converges, the implicit control function method of Steger and Sorenson involves curvature correction implicitly.

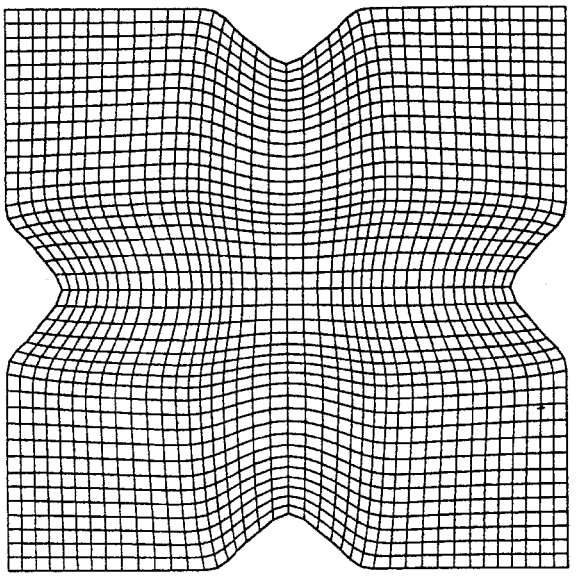

Fig. 12 Resulting grids of a smooth region, generated by Eqs. (5a), (7), (16), (21), (25), (29), and (30) and the algebraic advancing front method is employed to estimate boundary ϕ, ψ.

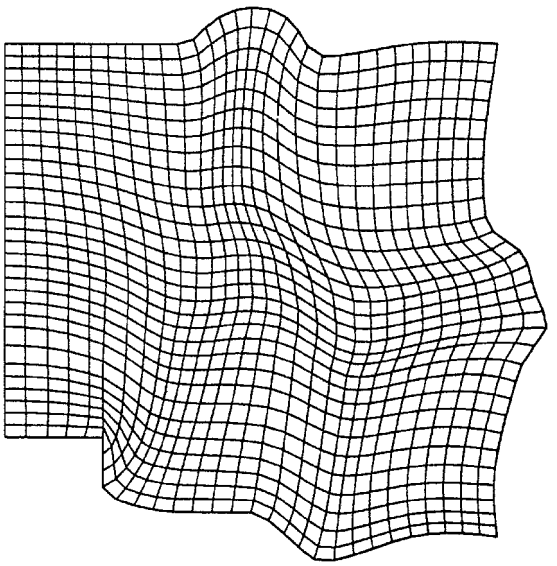

Fig. 13 Resulting grids of a relatively complicated region, generated by Eqs. (5a), (7), (16), (21), (25), (29), and (30) and the algebraic advancing front method is employed to estimate boundary ϕ, ψ.

Conclusions

A local curvature correction to the elliptic grid solver, which is an extension of Thompson's explicit method of specifying control function via the boundary curvature, is discussed in this study. The present method is helpful in improving grid smoothness for both linear and nonlinear grid systems with explicit control functions. For linear grid system where the interchange between the dependent and independent variables of the grid equation is not necessary, the present method requires a lengthy trial-and-error procedure and is not recommended. However, in the nonlinear systems corresponding to the original Thomas and Middlecoff method, the proposed curvature correction can improve grid smoothness easily and significantly, especially if boundary orthogonality is provided by several grid levels generated by the algebraic advancing front method.

References

[1]Thompson, J. F., Thames, F. C., and Mastin, C. W., "Boundary-Fitted Coordinate Systems for Numerical Solution of Partial Differential Equations—A Review," *Journal of Computational Physics*, Vol. 47, No. 1, 1982, pp. 1–108.

[2]Thompson, J. F., "A Survey of Dynamically Adaptive Grids in the Numerical Solution of Partial Differential Equations," *Applied Numerical Mathematics*, Vol. 1, No. 1, 1985, pp. 3–27.

[3]Thompson, J. F., and Weatherill, N. P., "Aspects of Numerical Grid Generation: Current Science and Art," AIAA Paper 93-3539, Aug. 1993.

[4]Thompson, J. F., "A Reflection on Grid Generation in the 90s: Trends, Needs, and Influences," *5th International Conference on Numerical Grid Generation in Computational Field Simulations*, edited by B. K. Soni, J. F. Thompson, F. Hauser, and P. Eiseman, Mississipi State Univ., Mississippi State, MS, 1996, pp. 1029–1109.

[5]Thompson, J. F., Warsi, Z. U. A., and Mastin, C. W., "Elliptic Generation Systems," *Numerical Grid Generation: Foundations and Applications*, edited by J. F. Thompson, Z. U. A. Warsi, and C. W. Mastin, North-Holland, Amsterdam, 1985, Chap. 6, pp. 188–263.

[6]Thompson, J. F., "Elliptic Grid Generation," *Numerical Grid Generation*, edited by J. F. Thompson, North-Holland, Amsterdam, 1982, pp. 79–105.

[7]Anderson, D. A., Tannehill, J. C., and Pletcher, R. H., "Grid Generation," *Computational Fluid Mechanics and Heat Transfer*, edited by D. A. Anderson, J. C. Tannehill, and R. H. Pletcher, Hemisphere, New York, 1984, pp. 519–546.

[8]Winslow, A. J., "Numerical Solution of the Quasilinear Poisson Equation in a Non-Uniform Triangle Mesh," *Journal of Computational Physics*, Vol. 1, No. 2, 1966, pp. 149–172.

[9]Thompson, J. F., Thames, F. C., and Mastin, C. W., "Automatic Numerical Generation of Body-Fitted Curvilinear Coordinate System for Field Containing any Number of Arbitrary Two-Dimensional Bodies," *Journal of Computational Physics*, Vol. 15, No. 3, 1974, pp. 299–312.

[10]Thompson, J. F., Thames, F. C., and Mastin, C. W., "TOMCAT—A Code for Numerical Generation of Boundary-Fitted Curvilinear Coordinate Systems on Fields Containing Any Number of Arbitrary Two-Dimensional Bodies," *Journal of Computational Physics*, Vol. 24, No. 3, 1977, pp. 274–302.

[11]Steger, J. L., and Sorenson, R. L., "Automatic Mesh-Point Clustering near a Boundary in Grid Generation with Elliptic Partial Differential Equations," *Journal of Computational Physics*, Vol. 33, No. 3, 1979, pp. 405–410.

[12]Sorenson, R. L., "A Computer Program to Generate Two-Dimensional Grid About Airfoil and Other Shapes by the Use of Poisson's Equation," NASA TM-81198, May 1980.

[13]Sorenson, R. L., "Three-Dimensional Elliptic Grid Generation About Fighter Aircraft for Zonal Finite-Difference Computations," AIAA Paper 86-0429, Jan. 1986.

[14]Shieh, C. F., "Three-Dimensional Grid Generation Using Elliptic Equations with Direct Grid Distribution Control," *AIAA Journal*, Vol. 22, No. 3, 1984, pp. 361–364.

[15]Hsu, K., and Lee, S. L., "A Numerical Technique for Two Dimensional Grid Generation with Grid Control at All of the Boundaries," *Journal of Computational Physics*, Vol. 96, No. 2, 1991, pp. 451–469.

[16]Jeng, Y. N., and Liou, Y. C., "Two Modified Versions of Hsu-Lee's Elliptic Solver of Grid Generation," *Numerical Heat Transfer, Part B*, Vol. 22, No. 2, 1992, pp. 125–140.

[17]Jeng, Y. N., and Liou, Y. C., "A New Adaptive Grid Generation by Elliptic Equations with Orthogonality at All of the Boundaries," *Journal of Scientific Computation*, Vol. 7, No. 1, 1992, pp. 63–80.

[18]Thomas, P. D., and Middlecoff, J. F., "Direct Control of the Grid Point Distribution in Meshes Generated by Elliptic Equations," *AIAA Journal*, Vol. 18, No. 6, 1980, pp. 652–656.

[19]Liou, Y. C., and Jeng, Y. N., "Algebraic Grid Front Marching Method," *Numerical Heat Transfer, Part B*, Vol. 28, No. 3, 1995, pp. 239–255.

[20]Jeng, Y. N., and Liou, Y.-C., "Hyperbolic Equation Method of Grid Generation for Enclosed Regions," *AIAA Journal*, Vol. 34, No. 6, 1996, pp. 1293–1295.

[21]Liou, Y. C., and Jeng, Y. N., "The Parabolic Equation Method of Grid Generation for Enclosed Regions," *Numerical Heat Transfer, Part B*, Vol. 29, No. 3, 1996, pp. 289–303.

[22]Visbal, M., and Knight, D., "Generation of Orthogonal and Nearly Orthogonal Coordinates with Grid Control near Boundaries," *AIAA Journal*, Vol. 20, No. 3, 1982, pp. 305, 306.

[23]Ryskin, G., and Leal, L. G., "Orthogonal Mapping," *Journal of Computational Physics*, Vol. 50, No. 1, 1983, pp. 71–100.

[24]Arina, R., "Orthogonal Grids with Adaptive Control," *1st International Conference on Numerical Grid Generation in CFD*, edited by J. Hauser and C. Taylor, Pineridge, Swansea, Wales, U.K., 1986, pp. 113–123.

[25]Duraiswami, R., and Prosperetti, A., "Orthogonal Mapping in Two Dimensions," *Journal of Computational Physics*, Vol. 98, No. 2, 1992, pp. 254–268.

[26] Albert, M. R., "Orthogonal Curvilinear Coordinate Generation for Internal Flows," *Numerical Grid Generation in Computational Fluid Mechanics*, Pineridge, Swansea, Wales, U.K., 1988, pp. 425–434.

[27] Allievi, A., and Calisal, S. M., "Application of Bubnov–Galerkin Formulation to Orthogonal Grid Generation," *Journal of Computational Physics*, Vol. 98, No. 1, 1992, pp. 163–173.

[28] Eça, L., "2D Orthogonal Grid Generation with Boundary Point Distribution Control," *Journal of Computational Physics*, Vol. 125, No. 2, 1996, pp. 440–453.

[29] Spekreijse, S. P., "Elliptic Grid Generation Based on Laplace Equations and Algebraic Transformations," *Journal of Computational Physics*, Vol. 118, No. 1, 1995, pp. 38–61.

[30] Thompson, J. F., "A General Three-Dimensional Elliptic Grid Generation System on a Composite Block Structure," *Computer Methods in Applied Mechanics and Engineering, Part B. Mesh Generation and Rezoning*, Vol. 64, Nos. 1–3, 1987, pp. 377–411.

[31] Eiseman, P. R., "Adaptive Grid Generation," *Computer Methods in Applied Mechanics and Engineering, Part B. Mesh Generation and Rezoning*, Vol. 64, Nos. 1–3, 1987, pp. 321–376.

J. Kallinderis
Associate Editor